PHYSICAL REVIEW B VOLUME 27, NUMBER 1 1 JANUARY 1983

Double sine-Gordon chain

C. A. Condat,* R. A. Guyer, and M. D. Miller
Laboratory for Low Temperature Physics, Department of Physics and Astronomy, Hasbrouck Laboratory, University of Massachusetts, Amherst, Massachusetts 01003
(Received 8 April 1982)

The thermodynamic properties of the double sine-Gordon chain are studied both analytically and numerically. Particular attention is given to the regime in which there are two different kinks (small and large) on the chain. The shape and energy of kinks are found in the continuum approximation. Comparison is made with numerical determination of the kink energies. The free energy, entropy, etc. of the chain are found. They are dominated by the small kinks. To see evidence for the participation of the large kinks the fluctuation in chain position and its equation of state are examined. The current carried by the chain is calculated. An unusual polarization precursor to activated conductivity is found. The polarization precursor is determined by the small kinks; the conductivity is determined by the large kinks.

I. INTRODUCTION

The thermodynamic properties of the sine-Gordon (SG) chain have been treated extensively.[1–6] Of particular importance is the low-temperature regime in which the solitons play a dominant role in the determination of the properties of the chain.

A closely related problem is that of the double sine-Gordon (DSG) chain, which has been shown to model several physical systems, e.g., the spin dynamics in the B phase of superfluid ^{3}He,[7] some features of the propagation of resonant ultrashort optical pulses through degenerate media,[8] nonlinear excitations in a compressible chain of XY dipoles under conditions of piezoelectric coupling,[9] macromolecules, etc.

In this paper we analyze the equilibrium and nonequilibrium properties of the DSG chain. For certain values of the parameter η characterizing the DSG potential two classes of kinks are present on the chain. This property endows the DSG chain with features that are qualitatively different from those of the sine-Gordon chain. Particular attention is paid to these new features.

In Sec. II we review the properties of the DSG chain that are the subject of this investigation. In Sec. III we present the Hamiltonian describing the DSG chain and derive the equation of the motion, which is then integrated to yield various types of localized nonlinear excitations. The energies associated with these excitations are also obtained. In Sec. IV we formulate the equilibrium thermodynamics using the transfer-integral technique. The problem of the calculation of the partition function is reduced to the problem of finding the eigenvalue spectrum of a transfer integral. This problem can be reduced further to the problem of a Schrödinger-type differential equation in the important case of strong coupling and low temperatures. This case is treated in detail in Sec. V, where the band structure of the eigenvalue spectrum of the differential equation is described using a tight-binding approximation. The thermodynamic functions are explicitly calculated in the various cases, and special attention is given to those properties (external torque, phase fluctuations) associated with the kinks. In Sec. VI, we consider the nonequilibrium problem resulting when the DSG chain is subject to a uniform external field. The phase current and the polarization found from the numerical solution to the transfer integral current problem are discussed. Analytic and numerical results are compared throughout.

II. THE DOUBLE SINE-GORDON CHAIN: A REVIEW OF ITS QUALITATIVE BEHAVIOR

In this section we describe the qualitative properties of the double sine-Gordon chain. The various properties that we describe are analyzed quantita-

tively both analytically and numerically in the sections that follow. The analytic work employs the equation of motion for particles on a discrete chain and the continuum approximation to this equation of motion; i.e., it employs the equation of motion for the phase at x, $\theta(x)$,

$$\ddot{\theta}-c^2\theta_{xx}+\left[\frac{c}{d}\right]^2(\sin\theta+2\eta\sin2\theta)=0\ , \qquad (2.1)$$

that follows from the energy

$$H[\theta]=\int dx\,\rho\left[\tfrac{1}{2}I\dot{\theta}^2-V_1(\cos\theta+\eta\cos2\theta)+\frac{\Gamma}{2}\theta_x^2\right], \qquad (2.1)$$

where $c^2=\Gamma/I$, $d^2=\Gamma/V_1$, and ρ is the linear-particle density. The energy in terms of the phase at site i, θ_i $(i=1,\ldots,M+1)$, is given by

$$H=\sum_{i=1}^{M}\left[\tfrac{1}{2}I\dot{\theta}_i^2-V_1(\cos\theta_i+\eta\cos2\theta_i)+\frac{\Gamma a^2}{2}(\theta_{i+1}-\theta_i)^2\right] \qquad (2.2)$$

and the corresponding equation of motion. The numerical work will employ only the discrete energy.

A. η and regions I, II, and III

Depending upon the value of η, the single-particle potential,

$$V(\theta)=-V_1(\cos\theta+\eta\cos2\theta)\ ,$$

has one of three shapes [Eq. (2.1)]. These shapes shown in Figs. 1–5 define regions I, II, and III. The critical values of η that separates regions of different shape are associated with the curvature of $V(\theta)$ at $\theta=0$ and $\theta=\pi$.

At $\theta=0$,

$$[V(\theta)/V_1]=-(1+\eta)+\theta^2(2\eta+\tfrac{1}{2})\ ,$$

and this curvature changes sign at $\eta=-\frac{1}{4}$; the boundary I-II is at $\eta=-\frac{1}{4}$.

At $\theta=\pi$,

$$[V(\theta)/V_1]=-(-\cos\phi+\eta\cos2\phi)\ ,$$

where $\theta=\pi+\phi$ and

$$[V(\phi)/V_1]=1-\eta+\phi^2(-\tfrac{1}{2}+2\eta)\ ,$$

where the curvature changes sign at $\eta=+\frac{1}{4}$; the boundary II-III is at $\eta=+\frac{1}{4}$. The kinds of kinks that can be present on the chain are different in regions I, II, and III.

B. Kinks in regions I, II, and III

The kind of kinks that are possible in each of the regions shown in Fig. 1 can be found from integration of the equation of motion, Eq. (2.1), by quadrature. In carrying through such a procedure one finds that the kinks correspond to the possible time-local motions of a particle in the potential $-V(\theta)$. This is shown in Fig. 2 where the potentials $-V(\theta)$ for regions I, II, and III are shown along with an energy diagram for the time-local motions to which the kinks correspond. In region I there are two kinds of kinks, a small kink denoted by $<$ and a large kink denoted by $>$. In region II there is one kink which at $\eta=0$ is the sine-Gordon soliton (or antisoliton). In region III there is a kink and a critical bubble (or bounce). Figures 3–5 show the kink structure. Details are in Sec. III A.

C. Kink energies

The existence of kink solutions to Eq. (2.1) follows from the analysis of that equation remarked on above. Once the solution $\theta(x)$ for a particular kink is found it can be substituted into $H(\theta)$ and the energy of the kink determined. The physical mechanism that gives rise to the kink structure is the competition between the single-particle potential (that wants phase evolution to occur over as short a length of chain as possible) and the elastic energy

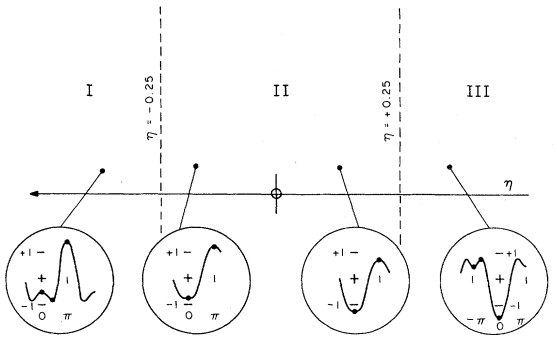

FIG. 1. η regions. As η in Eq. (2.1) varies the qualitative nature of the single-particle potential changes. The behavior of $V(\theta)$ is shown for regions I, II, and III (see below Eq. (2.2) and Eq. (3.2)).

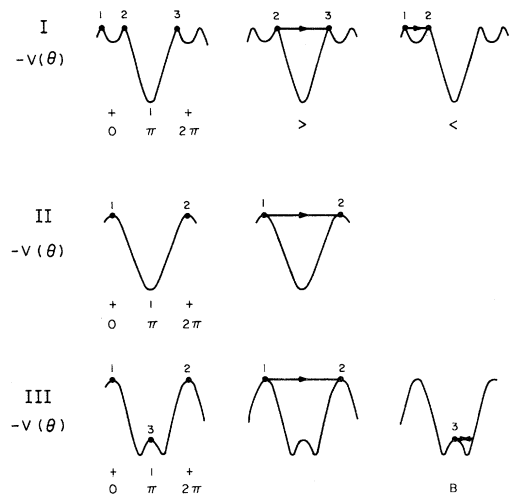

FIG. 2. Kinks. The solution to Eq. (2.1) or Eq. (3.3) is equivalent to the motion of a particle in $-V(\theta)$. In this picture the kinks correspond to motions that are local in time. There are two possible such motions in $-V(\theta)$ from region I: the large kink $2\rightarrow 3$ and the small kink $1\rightarrow 2$. In region III there are two local motions, the kink $1\rightarrow 2$ and the bubble $3\rightarrow 3$. See also Figs. 3–5.

(that wants the phase evolution to occur over as long a length of chain as possible).[2] Upon modeling this competition in terms of the height of the single-particle potential barrier, A, the strength of the elastic force, B, and the total phase evolution involved in producing the kink, Δ (see, e.g., the small kink in Figs. 2 or 3), it is easy to show that the energy of a kink scales as

$$E_\phi \propto \sqrt{AB}\,\Delta\ .$$

B, a measure of the elastic energy, is independent of η. Both A and Δ depend upon η. At $\eta=0$, the sine-Gordon kink, we have $A=2V_1$, $\Delta=2\pi$. In region I, for $\eta\simeq -0.25$ we have $A=-V_1[1-(1/8\,|\,\eta\,|\,)]$ and $\Delta=2\cos^{-1}(\frac{1}{4}\eta)$ for the small kink, etc. Thus the energy required to produce a kink is a complicated function of the η which determines the single-particle potential and phase evolution involved in the kink. See Figs. 3–5 and 7. Details are in Sec. III B.

D. Kinks or solitons

At $\eta=0$ the DSG chain reduced to the SG chain. The SG kinks are solitons in the strict sense[10]; they retain their integrity (including velocity) after collision with one another pairwise, etc. Extensive numerical work by the Manchester group[11] and Kumar and co-workers[7,12] has shown that the DSG kinks are not solitons. The radiation of phonons during collision signals their inelastic character and the evolution of a kink pair into a variety of final states.

E. DSG kinks in equilibrium statistical mechanics and dynamics

1. Statics

The DSG kinks are topological excitations; they can be at rest. To create them requires a rest energy, the kink energy from Sec. II C above. Thus the kinks will be seen in the equilibrium thermal properties of the chain through their Boltzmann factor signature $\exp(-\beta E_\phi)$. In region II the participation of the kinks in the equilibrium thermal properties will be much like that found for the sine-Gordon chain.[1–6] Region I will be more interesting because two rather different kinks are present. (For $\eta \ll -0.25$ the two kinds of kinks become almost similar in energy and structure.) Consider the behavior of the chain for $\eta \lesssim -0.25$. The kink most copiously present, the small kink (which always has less rest energy than the large kink, even at $\eta \ll -0.25$) will make itself known in the energy, in the entropy, in the specific heat, etc., through the Boltzmann factor $\exp(-\beta E_\phi^<)$ that determines $N^<$, the equilibrium number of these kinks. At low temperatures the free energy will be given by

$$F=F_0+N^<\Delta F(T,N^<)\ ,$$

where F_0 is the free energy of the kinkless chain. On one hand, the large kink will also be present but it will be hard to see its thermal signature, $\exp(-\beta E_\phi^>)$, against the background of small kinks. On the other hand, when phase evolution is involved it is accomplished by the creation of equal numbers of small and large kinks. Phase evolution from 0 to 2π requires one small and one large kink. Thus evidence for the presence of large kinks is found in the fluctuations, $\langle\theta(x)^2\rangle-\langle\theta(x)\rangle^2$, or in the total phase evolution, $\Phi=\langle\theta_{M+1}-\theta_1\rangle$, that results from application of a torque, the $\Phi-\tau$ relation, or equation of state. Details are in Secs. IV and V.

2. Dynamics

When each particle on the SG chain (or each piece of the chain) is subject to a constant external

torque a steady-state phase current results. This current has been the subject of a number of studies.[3,13] The feature that emerges from these studies is that, at low temperature and low external torque, the important current-carrying object is the sine-Gordon soliton, the kink. We expect the same qualitative result for the DSG chain. The torque drives the phase; the current that flows in response to this drive is a phase current. A phase current, a measure of the rate of phase evolution, corresponds to the rate of kink evolution, a kink current. The phase evolution of a typical piece of the chain might be $0\rightarrow 2\pi\rightarrow 4\pi\rightarrow\cdots$; i.e., the phase evolution must involve both the small and the large kinks. However, as there are many fewer large than small kinks the current $\overline{W}$ is governed by the number of large kinks,

$$\overline{W}\propto\exp(-\beta E_{\phi}^{>}) .$$

Details are in Sec. VI A.

There is a further consequence of the application of an external torque to the chain. An external torque produces a polarization of the chain. Between two large kinks spaced apart by

$$(N^{>})^{-1}\simeq\exp(\beta E_{\phi}^{>}) ,$$

there can be many small kinks, typically $N^{<}/N^{>}$. The external torque polarizes this small-kink region of the chain, $\langle\theta\rangle\neq 0$, etc. Details are in Sec. VI B.

III. THE KINKS

A. $\theta(x)$

In this section we discuss the stationary-wave solutions of the DSG equation (the kinks) and write down their energies. The structure of the kinks and their energies depend upon the parameter η, which characterizes the shape of the potential. We begin with the discrete DSG chain, whose Hamiltonian is written as

$$H=\sum_{i=1}^{M}\left[\tfrac{1}{2}I\dot{\theta}_i^2-E_1(\cos\theta_i+\eta\cos 2\theta_i)+\frac{E_2}{2}(\theta_{i+1}-\theta_i)^2\right] , \tag{3.1}$$

where θ_i and $\dot{\theta}_i$ are, respectively, the coordinate and angular velocity corresponding to the ith particle. It may be useful to think of the Hamiltonian (3.1) as representing a collection of physical pendula joined by torsion springs of strength E_2 and placed in an external potential equal to

$$-E_1(\cos\theta+\eta\cos 2\theta)$$

(Ref. 2); θ_i and $\dot{\theta}_i$ are then the displacement from equilibrium and the angular velocity of the ith pendulum, and I is its moment of inertia.

If a is the lattice constant (the spacing between the pendula) and ρ a suitably defined linear density, we can use the transformations

$$E_1\leftrightarrow\rho V_1$$

and

$$E_2\leftrightarrow\Gamma\rho/a^2$$

to write the continuum version of the Hamiltonian (3.1), which reads:

$$H=\int\left[\left[\frac{I}{2}\right]\dot{\theta}^2-V_1(\cos\theta+\eta\cos 2\theta)+\left[\frac{\Gamma}{2}\right]\theta_x^2\right]\rho\,dx , \tag{3.2}$$

where $\theta_x=\partial\theta/\partial x$.

The potential

$$V(\theta)=-V_1(\cos\theta+\eta\cos 2\theta)$$

has different behavior in each of the regions I, II, and III (shown in Fig. 1) determined by η.

(a) $\eta<-\frac{1}{4}$. The minima in $V(\theta)$ are located at the positions

$$\theta=\cos^{-1}(-\tfrac{1}{4}\eta)+2n\pi ,$$

for all integers n, and are all degenerate. There are absolute maxima at $\theta=(2n+1)\pi$ and relative maxima at $\theta=2n\pi$ (see Fig. 3). The equation for the spin dyamics in superfluid ^{3}HeB belongs in this region, having $\eta=-1$.[7]

(b) $|\eta|\leq\frac{1}{4}$. There are degenerate minima in $V(\theta)$ at $\theta=2n\pi$ and maxima at $\theta=(2n+1)\pi$ (see Fig. 4). The usual sine-Gordon chain, for which $\eta=0$, belongs in this region.

(c) $\eta>\frac{1}{4}$. There are absolute minima of $V(\theta)$ at $\theta=2n\pi$ and relative minima at $\theta=(2n+1)\pi$. These relative minima are called "false vacua" by Mason.[14] The maxima are located at

$$\theta=\cos^{-1}(-1/4\eta)+2n\pi$$

(see Fig. 5).

Defining $c^2=\Gamma/I$ and $d^2=\Gamma/V_1\equiv\xi^2a^2$, the equation of the motion corresponding to the Hamil-

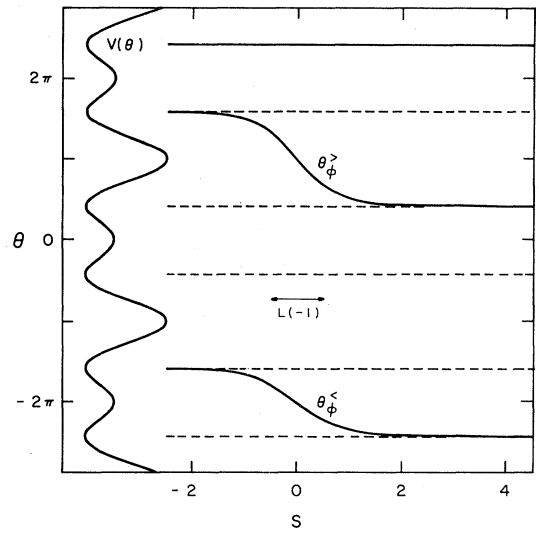

FIG. 3. Kinks in region I. The potential $V(\theta)$ for $\eta=-1$ is plotted at the left vs θ. In the right part of the Fig. $\theta(s)$ is plotted vs x for the undisturbed chain (up), for the large kink (middle), and for the small kink (down).

tonia (3.2) is

$$\ddot{\theta}-c^2\theta_{xx}+\left[\frac{c}{d^2}\right]^2(\sin\theta+2\eta\sin2\theta)=0\ . \tag{3.3}$$

Since we will be interested in the solutions to Eq. (3.3) that represent waves traveling with speed v, it

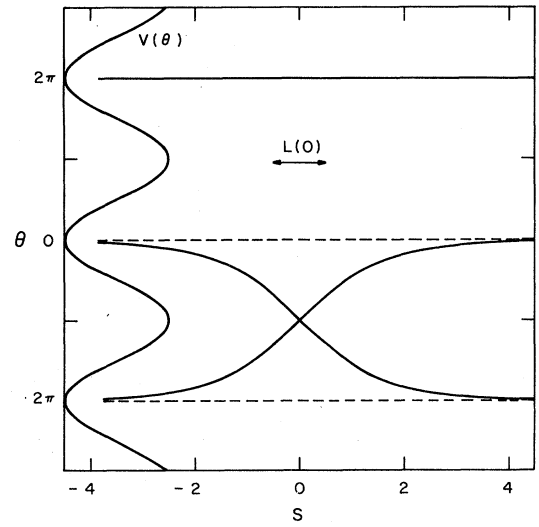

FIG. 4. Kinks in region II. The potential $V(\theta)$ for $\eta=0$ is plotted vs θ. In the right part of the figure $\theta(s)$ is plotted vs x for the kink (in this case $\eta=0$, a soliton) and the antikink (antisoliton).

is convenient to define $s=(\gamma/d)(x-vt)$, with $\gamma=[1-(v/c)^2]^{-1/2}$, and write Eq. (3.3) as

$$\theta_{ss}=\sin\theta+2\eta\sin2\theta\ . \tag{3.4}$$

The kinks $\theta_\phi(s)$ are the solutions of Eq. (3.4) which satisfy the boundary conditions $\theta_\phi(s=\pm\infty)=\theta_a,\theta_b$, $(d\theta_\phi/ds)$ $(s=\pm\infty)=0$. Here θ_a and θ_b are minima of $V(\theta)$. It is useful to note that Eq. (3.4) is the conventional equation of the motion for a particle of unit mass in the potential $+(\cos\theta+\eta\cos2\theta)$, that is, the motion of the kinks in the potential $V(\theta)$ can be thought of as the motion of classical particles in a potential $V'(\theta)=-V(\theta)$ (see Fig. 2).

Integrating Eq. (3.4) twice with the stated boundary conditions, we find that the kinks $\theta_\phi(s)$ satisfy the following equations.

(a) $\eta<-\frac{1}{4}$:

$$\tan\left[\frac{\theta_\phi^>}{2}\right]=\pm\left[\frac{4|\eta|-1}{4|\eta|+1}\right]^{1/2}\times\coth\left[\left[\frac{16|\eta|^2-1}{16|\eta|}\right]^{1/2}s\right] \tag{3.5}$$

and

$$\tan\left[\frac{\theta_\phi^<}{2}\right]=\pm\left[\frac{4|\eta|-1}{4|\eta|+1}\right]^{1/2}\times\tanh\left[\left[\frac{16|\eta|^2-1}{16|\eta|}\right]^{1/2}s\right]\ . \tag{3.6}$$

The solution $\theta_\phi^>(s)$, which we call the "large kink," links two minima across one of the absolute maxima at $\theta=(2n+1)\pi$, while the solution $\theta_\phi^<(s)$, the "small kink," links two minima across one of the relative maxima at $\theta=2n\pi$. These kinks are depicted in Figs. 2 and 3. The double signs in Eqs. (3.5) and (3.6) show explicitly the possibility of having kinks and antikinks.

(b) $|\eta|<\frac{1}{4}$:

$$\tan\left[\frac{\theta_\phi^>}{2}\right]=\pm(1+4\eta)^{-1/2}\,\mathrm{cosech}[(1+4\eta)^{1/2}s]\ . \tag{3.7}$$

The potential has the simple structure shown in Figs. 2 and 4, and we obtain only one type of kink,

which we call $\theta_\phi^>(s)$ because it goes continually to the solution (3.5) when η goes through $-\frac{1}{4}$.

(c) $\eta > \frac{1}{4}$.

$$\tan\left[\frac{\theta_\phi^>}{2}\right] = \pm(1+4\eta)^{-1/2}\,\mathrm{cosech}[(1+4\eta)^{1/2}s]\ . \tag{3.8}$$

This solution connects two absolute minima of $V(\theta)$. The wavy shape of the kink shown in Fig. 5 near the maximum $V(\theta)$ is due to the passage of the chain over these maxima and the intervening relative minimum. There are also solutions $\theta_\phi^B(s)$ which tend asymptotically to the same relative minimum when $s\to+\infty$ and $s\to-\infty$,

$$\tan\left[\frac{\theta_\phi^B}{2}\right] = \pm(4\eta-1)^{-1/2}\,\mathrm{sech}[(4\eta-1)^{1/2}s]\ . \tag{3.9}$$

This solution hangs over one of the maxima into the absolute minimum, as it is shown in Fig. 5. The point of its closest approach to the absolute minimum lies at

$$\theta = 2\tan^{-1}[(4\eta-1)^{1/2}]\ ,$$

the position at which the potential reaches the same value it has as the relative minimum. The unstable object described by Eq. (3.9) has been called a critical bubble.[14]

The dynamical behavior of the DSG kinks has been extensively studied by several groups.[11,12] These studies reveal that the collisions between kinks are not radiationless; therefore, the kinks described here do not qualify as solitons.

The argument of the hyperbolic function appearing in the equations above for a kink can be written in the form $\gamma(x-vt)/L(\eta)$, where $L(\eta)$ characterizes the length of a kink at rest. This proper length of the kinks is plotted in Fig. 6 as a function of η. For example, if $|\eta|<\frac{1}{4}$, $L(\eta)=(1+4\eta)^{-1/2}d$. Note that $L(\eta)$ gets larger and larger as we approach $\eta=-\frac{1}{4}$: Owing to the flatness of the potential, it takes the kink a long distance to reach the minimum. On the contrary, if $|\eta|$ is large the potential minima and maxima are sharp and $L(\eta)$ is small. The length of a moving kink is Lorentz-contracted to $L'(\eta)=L(\eta)/\gamma$.

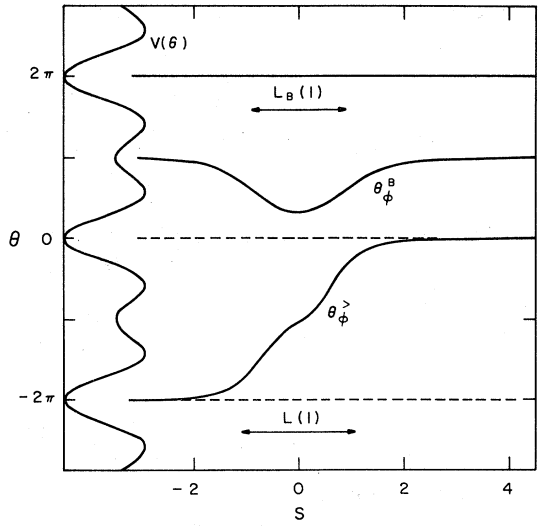

FIG. 5. Kinks in region III. The potential $V(\theta)$ for $\eta=+1$ is plotted vs θ. In the right part of the figure $\theta(s)$ is plotted vs x for the bubble (middle) and for the kink (down). For the bounce only a small part of the chain is not at large potential energy. The "anomalous" slope of $\theta_\phi^>$ has been exaggerated for the sake of clarity.

B. The energy

From Eq. (3.2) and Eqs. (3.5)–(3.9) it is easy to obtain the kink energies $E(\eta)$. We express these in terms of $E_\phi^>(0)=8\sqrt{E_1E_2}=8\sqrt{V_1\Gamma\rho}$, the rest energy of the usual sine-Gordon soliton.

(a) $\eta<-\frac{1}{4}$:

$$E_\phi^>(\eta)=\gamma[E_\phi^>(0)/8\,|\eta|^{1/2}][(16\eta^2-1)^{1/2}+\pi-\cos^{-1}(\tfrac{1}{4}|\eta|)]\ , \tag{3.10}$$

$$E_\phi^<(\eta)=\gamma[E_\phi^>(0)/8\,|\eta|^{1/2}][(16\eta^2-1)^{1/2}-\cos^{-1}(\tfrac{1}{4}|\eta|)]\ . \tag{3.11}$$

(b) $|\eta|\le\frac{1}{4}$:

$$E_\phi^>(\eta)=\begin{cases}\gamma[E_\phi^>(0)/4\,|\eta|^{1/2}][2\,|\eta|^{1/2}(1+4\eta)^{1/2}+\sin^{-1}(2\,|\eta|^{1/2})], & \eta\le 0 \qquad (3.12)\\ \gamma[E_\phi^>(0)/4\eta^{1/2}]\{2\eta^{1/2}(1+4\eta)^{1/2}+\ln[(1+4\eta)^{1/2}+2\eta^{1/2}]\}, & \eta\ge 0\ . \qquad (3.13)\end{cases}$$

Note that when $\eta \to 0$, both Eqs. (3.12) and (3.13) go to the sine-Gordon limit.

(c) $\eta > \frac{1}{4}$:

$$E_\phi^>(\eta) = \gamma[E_\phi^>(0)/4\eta^{1/2}]\{2\eta^{1/2}(1+4\eta)^{1/2} + \ln[(1+4\eta)^{1/2}+2\eta^{1/2}]\} , \tag{3.14}$$

$$E_\phi^B(\eta) = \gamma[E_\phi^>(0)/4\eta^{1/2}]\{2\eta^{1/2}(4\eta-1)^{1/2} - \ln[(4\eta-1)^{1/2}+2\eta^{1/2}]\} . \tag{3.15}$$

The factor γ in Eqs. (3.10)–(3.15) shows explicitly the relativistic form of the energy. It is interesting to note that

$$E_\phi^>(\eta \to +\infty),\ E_\phi^B(\eta \to +\infty) \sim \gamma E_\phi^>(0)\eta^{1/2} ,$$

but

$$E_\phi^>(\eta \to -\infty),\ E_\phi^<(\eta \to -\infty) \sim \gamma E_\phi^>(0)\,|\eta|^{1/2}/2 .$$

This factor of $\frac{1}{2}$ arises because the kinks $\theta_\phi^>$ and $\theta_\phi^<$ span only a phase of π, while the two types of minima found in case (c) are nondegenerate for any finite value of η and thus both $\theta_\phi^>(\eta)$ and $\theta_\phi^B(\eta)$ must span a phase of 2π when $\eta \to \infty$.

IV. EQUILIBRIUM STATISTICAL MECHANICS

In this section we present the formalism which will be used in Sec. V to compute the thermodynamic properties of the DSG chain in the strong-coupling, low-temperature limit. The partition function for a DSG chain containing $M+1$ particles (pendula) and embedded in a temperature reservoir at temperature T is

$$Z(T,\Phi) = (2\pi k_B T/I)^{(M-1)/2} Z_v , \tag{4.1}$$

where we have made explicit the dependence of the partition function on the total phase Φ, which is defined by

$$\Phi = \sum_{i=1}^{M} (\theta_{i+1}-\theta_i) = \theta_{M+1}-\theta_1 , \tag{4.2}$$

and is due to the applied torque τ. We write the constraints on the partition function as $\theta_1 = \Theta$, $\theta_{M+1} = \Phi + \Theta$, with $\Theta = 0$ if $\eta > -0.25$ and $\Theta = |\cos^{-1}(\frac{1}{4}|\eta|)|$ if $\eta < -0.25$. In the last case, the first particle is therefore constrained to be at the bottom of the right-hand well in the first unit cell. The configurational partition function is

$$Z_v = \int d\theta_1 \cdots d\theta_{M+1} \delta(\theta_1 - \Theta) \times \delta(\theta_{M+1} - \Phi - \Theta) e^{-\beta V(\theta_1,\ldots,\theta_{M+1})} , \tag{4.3}$$

with

$$V(\theta_1,\ldots,\theta_{M+1}) = \sum_{i=1}^{M+1} [-E_1(\cos\theta_i + \eta\cos 2\theta_i) + (E_2/2)(\theta_{i+1}-\theta_i)^2] . \tag{4.4}$$

The thermodynamic properties of the system can be obtained from Eq. (4.1). The Helmholtz free energy is

$$F(T,\Phi) = -k_B T \ln Z(T,\Phi) . \tag{4.5}$$

Since $dF = -S\,dT - \tau d\Phi$, the entropy S and the torque τ are given by

$$S = -\left[\frac{\partial F}{\partial T}\right]_\Phi \tag{4.6}$$

and

$$\tau = -\left[\frac{\partial F}{\partial \Phi}\right]_T . \tag{4.7}$$

Other quantities of interest are the internal energy,

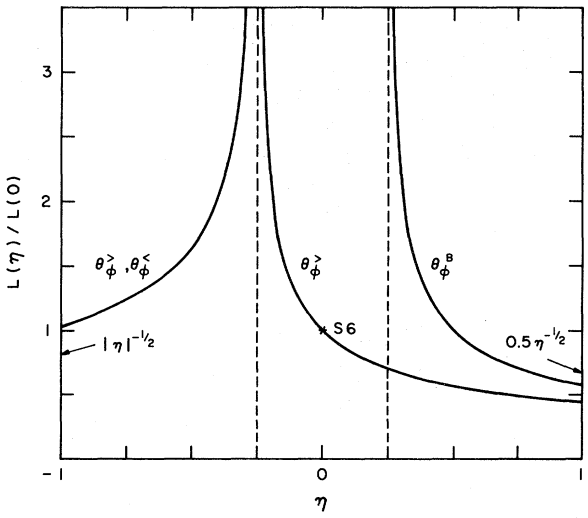

FIG. 6. Kink length. The proper length of the kink is plotted as a function of η (in units of the proper length at $\eta = 0$). The asymptotic behavior for large $|\eta|$ is shown. This length is a measure of how much of the chain is involved in the kink structure.

$$U=F+TS\ , \tag{4.8}$$

and the specific heat at constant length,

$$C_v=\left[\frac{\partial U}{\partial T}\right]_{\Phi}\ . \tag{4.9}$$

We will evaluate Z_v using a complete set of orthonormal states $\{\psi_\nu(\theta)\}$, whose completeness relation

$$\delta(\theta-\theta')=\sum_\nu \phi_\nu(\theta)\psi_\nu(\theta') \tag{4.10}$$

allows us to write

$$Z_v=\sum_{\mu\nu}\int d\theta_1,\ldots d\theta_{M+1}\,\phi_\nu(\Phi+\Theta)\psi_\mu(\Theta)\phi_\mu(\theta_1) \times e^{-\beta V(\theta_1,\ldots,\theta_{M+1})}\psi_\nu(\theta_{M+1})\ . \tag{4.11}$$

We choose ψ_ν and ϕ_ν to be the right- and left-hand eigenfunctions of the transfer integral problem[15,16]

$$\int d\theta_{i+1}e^{-K(\theta_i,\theta_{i+1})}\psi_\nu(\theta_{i+1})=e^{-\beta\epsilon_\nu}\psi_\nu(\theta_i)\ , \tag{4.12}$$

$$\int d\theta_i\phi_\nu(\theta_i)e^{-K(\theta_i,\theta_{i+1})}=e^{-\beta\epsilon_\nu}\phi_\nu(\theta_{i+1})\ , \tag{4.13}$$

with

$$K(\theta_i,\theta_{i+1})=-\lambda_1(\cos\theta_i+\eta\cos2\theta_i) +(\lambda_2/2)(\theta_{i+1}-\theta_i)^2\ , \tag{4.14}$$

where $\lambda_1=\beta E_1$ and $\lambda_2=\beta E_2$. Repeated use of Eq. (4.12) in Eq. (4.11) leads to

$$Z_v=\sum_\nu \phi_\nu(\Phi+\Theta)\psi_\nu(\Theta)e^{-M\beta\epsilon_\nu}\ . \tag{4.15}$$

If we were using periodic boundary conditions, i.e., $\theta_1=\theta_{M+1}$, it would be simpler to symmetrize the kernel and work with only one set of eigenfunctions. However, since we intend to study the system when it is acted upon by an external torque and the isotropy of the chain is broken, we are forced to keep explicitly different right-hand and left-hand eigenfunctions. By inspection of Eqs. (4.12) and (4.13), we see that these eigenfunctions are related by

$$\phi_\nu(\theta)=e^{\lambda_1(\cos\theta+\cos2\theta)}\psi_\nu^*(\theta)\ . \tag{4.16}$$

The single-particle and two-particle averages can be readily obtained as[15,16]

$$\langle f(\theta_{j+1})\rangle=\frac{1}{Z_v}\sum_{\mu\nu}\phi_\nu(\Phi+\Theta)\psi_\mu(\Theta)f_{\mu\nu} \times e^{-(M-j)\beta\epsilon_\nu}e^{-j\beta\epsilon_\mu}\ , \tag{4.17}$$

with

$$f_{\mu\nu}=\int d\theta\phi_\mu(\theta)F(\theta)\psi_\nu(\theta)\ , \tag{4.18}$$

$$\langle f(\theta_{j+1})g(\theta_{k+1})\rangle=\frac{1}{Z_v}\sum_{\mu\nu\nu'}\phi_\nu(\Phi+\Theta)\psi_\mu(\Theta)f_{\mu\nu'}g_{\nu'\nu}e^{-(M-j)\beta\epsilon_\nu}e^{-(j-k)\beta\epsilon_{\nu'}}e^{-k\beta\epsilon_\mu}\ . \tag{4.19}$$

Our problem has been reduced to the calculation of the solution to the transfer-integral problem defined by Eqs. (4.12) and (4.13), i.e.,

$$\int_{-\infty}^{\infty}d\theta_{i+1}e^{\lambda_1(\cos\theta_i+\eta\cos2\theta_i)}e^{-\lambda_2(\theta_{i+1}-\theta_i)^2/2}\psi_\nu(\theta_{i+1})=e^{-\beta\epsilon_\nu}\psi_\nu(\theta_i)\ . \tag{4.20}$$

Using a cumulant expansion[2] we cast Eq. (4.20) in a differential form,

$$e^{\lambda_1(\cos\theta+\eta\cos2\theta)}e^{D^2/2\lambda_2}\psi_\nu(\theta)=e^{-\beta\tilde{\epsilon}_\nu}\psi_\nu(\theta)\ , \tag{4.21}$$

where $D\equiv d/d\theta$ and $\beta\tilde{\epsilon}_\nu=\beta\epsilon_\nu-\frac{1}{2}\ln(\lambda_2/2\pi)$. Two simple special cases are as follows.

(a) $E_2=0$. The pendula are independent and Eq. (4.20) yields

$$\psi(\theta_i)=e^{\lambda_1(\cos\theta_i+\eta\cos2\theta_i)}\ . \tag{4.22}$$

(b) $E_1=0$. We have an $(M+1)$-particle elastic band or a piece of spring steel, and Eq. (4.21) reduces to the differential equation

$$-\frac{1}{2\lambda_2}\frac{d^2}{d\theta^2}\psi_\nu(\theta)=\beta\tilde{\epsilon}_\nu\psi_\nu(\theta)\ , \tag{4.23}$$

with $\beta\tilde{\epsilon}=\nu^2/2\lambda_2$, and

$$\phi_\nu(\theta)=\psi_\nu^*(\theta)=(2\pi)^{-1/2}e^{-i\nu\theta}\ .$$

The thermodynamic properties of the system described by Eq. (4.23) have already been discussed.[1,2]

A more interesting case of Eqs. (4.20) and (4.21) occurs when $\lambda_2 \gg \lambda_1 \gg 1$: the torsion spring is much stronger than the external potential, while the reservoir temperature is low as compared to the height of the periodic barrier. The phase evolution occurs over a large number of sites and a good approximation to the solution of Eq. (4.21) can be obtained from the associated differential equation[1,2]

$$\left[-\frac{1}{2\lambda_2}\frac{d^2}{d\theta^2}-\lambda_1(\cos\theta+\eta\cos 2\theta)\right]\psi_\nu(\theta)=\beta\tilde{\epsilon}\psi_\nu(\theta)\ . \tag{4.24}$$

If $\eta=0$, this is Mathieu's equation. Below we study the equilibrium statistical mechanics of the DSG chain in the strong-coupling limit using Eq. (4.24) and the collection of formulas recorded here.

V. EQUILIBRIUM STATISTICAL MECHANICS IN THE STRONG-COUPLING REGIME

In this section we discuss the properties of the DSG system in the low-temperature, strong-coupling regime. Particular attention is paid to the torque and displacement fluctuations, which are sensitive to the behavior of the kinks on the chain. According to Eq. (4.15) the thermodynamic properties can be determined from a knowledge of the eigenvalue spectrum of the transfer integral Eq. (4.12). In the strong-coupling regime we replace Eq. (4.12) by the Schrödinger-equation approximation, Eq. (4.24). We describe the behavior of the eigenvalue spectrum of Eq. (4.12) and use of that eigenvalue spectrum in Eq. (4.15) and related equations to learn about the thermodynamic properties. Two cases are treated, $\eta<-\frac{1}{4}$, where two types of kinks are present, and $\eta>-\frac{1}{4}$, where there is only one kink and the thermodynamic properties are much like those of the sine-Gordon chain.

A. $\eta<-\frac{1}{4}$

In this case the potential $V(\theta)$ has the form shown in Figs. 1 and 3. First, let us determine the ground-state energy level $\tilde{\epsilon}_{00}$ corresponding to a single well. This is done by taking a quadratic approximation to the potential near the bottom of the well; the first energy level is therefore the ground state of a harmonic oscillator. We then use perturbation theory to include the contribution of the anharmonic terms. We obtain

$$\begin{aligned}\beta\tilde{\epsilon}_{00}=-\lambda_1\{\ &|\eta|+\tfrac{1}{8}|\eta| \\ &-[(16|\eta|^2-1)/16|\eta|\lambda_1\lambda_2]^{1/2} \\ &+(64|\eta|^2-7)/32(16|\eta|^2-1)\lambda_1\lambda_2\}\ .\end{aligned} \tag{5.1}$$

Equation (5.1) suffices to evaluate the main contributions to certain thermodynamic functions, e.g., the entropy and the specific heat, at very low temperatures. However, to calculate those quantities associated with the overall behavior of the chain, e.g., its length, fluctuations, etc., we need to have some knowledge of the kinks. These make themselves known through the band structure. Under the conditions we are interested in, the tight-binding approach presented in detail in Appendix A gives us the essential features that are called for. The tight-binding bands are given by Eq. (A8), and

$$\tilde{\epsilon}_\nu^{\pm}=\tilde{\epsilon}_{00}\pm(t_1^2+t_2^2+2t_1t_2\cos 2\pi\nu)^{1/2}\ , \tag{5.2}$$

where t_1 and t_2 are the tunneling rates through the small and large barriers, respectively. At low temperatures only the "minus" band will be relevant. The bands are shown in Fig. 7. A satisfactory estimate of the tunneling rates that go into Eq. (5.2) can be obtained using the Wentzel-Kramers-Brillouin (WKB) approximation, which yields the formula[8]

$$t_i=\frac{E(T)}{\pi}e^{-P_i(\eta)}\ , \tag{5.3}$$

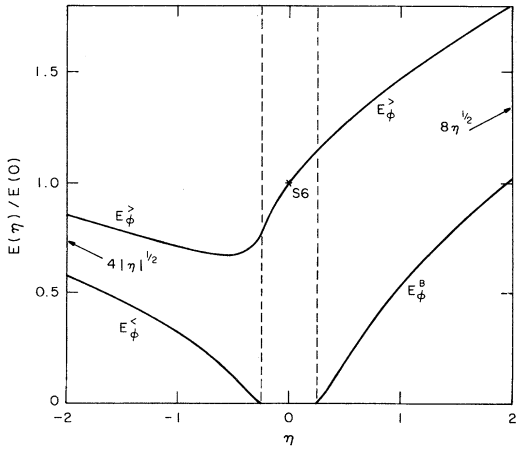

FIG. 7. Kink energy. The kink rest energy is plotted as a function of η (in units of the $\eta=0$ kink energy, the sine-Gordon kink energy). Note the different asymptotic limits as $\eta\to+\infty$ and $\eta\to-\infty$.

with

$$P_i(\eta)=(2\lambda_2)^{1/2} \times \int_{a_i}^{b_i}[\beta E(T)+\lambda_1(\cos\theta+\eta\cos2\theta)]^{1/2}d\theta\ , \tag{5.4}$$

where

$$\beta E(T)=[(16\,|\,\eta\,|^2-1)/16\,|\,\eta\,|\,]^{1/2}(\lambda_1/\lambda_2)^{1/2} \tag{5.5}$$

is the appropriate harmonic-oscillator ground-state energy measured from the bottom of the well [see Eq. (5.1)], and a_i and b_i are the turning points for the barrier characterized by the tunneling rate t_i (cf. Fig. 15). The numerical value of the WKB prefactor in Eq. (5.3) can be improved,[17] but the most important feature of Eq. (5.2) is the relationship between its exponent and the static kink energies. One can verify by an explicit calculation of the integral in Eq. (5.4) that

$$P_1=\beta E_\phi^<(\eta),\quad P_2=\beta E_\phi^>(\eta)\ . \tag{5.6}$$

The tight-binding wave function can be written as

$$\psi_\nu(\theta)=(2\pi)^{-1/2}\sum_j e^{i2\pi\nu j}[\chi_0(\theta-2\pi j-\Theta)+\chi_0(\theta-2\pi j+\Theta)]\ , \tag{5.7}$$

where $\chi_0(\theta-2\pi j-\Theta)$ and $\chi_0(\theta-2\pi j+\Theta)$ are functions strongly localized near the right- and left-hand minima of the jth cell, respectively. (See Appendix B.) We can use these results and Eq. (4.16) to obtain an expression for the configurational partition function, Eq. (4.15),

$$Z_v=(1/2\pi)e^{-\lambda_1[\,|\,\eta\,|+1/8\,|\,\eta\,|\,]}\,|\,\chi_0(0)\,|^2 e^{-(M/2)\ln(\lambda_2/2\pi)}e^{-M\beta\tilde{\epsilon}_{00}}\int_{-1/2}^{1/2}e^{-2\pi iN\nu}e^{M\beta(t_1^2+t_2^2+2t_1t_2\cos2\pi\nu)^{1/2}}d\nu\ . \tag{5.8}$$

Using Eq. (B9), we can write the total partition function as

$$Z=(2\pi k_BT/I)^{(M-1)/2}[\lambda_1\lambda_2(\,|\,\eta\,|-1/16\,|\,\eta\,|\,)/4\pi^2]^{1/4}e^{-(M/2)\ln(\lambda_2/2\pi)}e^{-M\beta\tilde{\epsilon}_{00}}J_M(N;t_1,t_2)\ , \tag{5.9}$$

with

$$J_M(N;t_1,t_2)=(1/2\pi)\int_{-\pi}^{\pi}e^{-iNx}e^{M\beta(t_1^2+t_2^2+2t_1t_2\cos x)^{1/2}}dx\ . \tag{5.10}$$

Therefore, the free energy is

$$F(T,\Phi)=F_0(T,0)+\Delta F(T,\Phi)\ , \tag{5.11}$$

where

$$F_0(T,0)=\frac{k_BT}{4}\ln\left[\frac{(2\pi k_BT)^4}{I^2E_1E_2(\,|\,\eta\,|-1/16\,|\,\eta\,|\,)}\right]-k_BTM\ln\left[\frac{2\pi k_BT}{(IE_2)^{1/2}}\right]+M\tilde{\epsilon}_{00} \tag{5.12}$$

and

$$\Delta F(T,\Phi)=-k_BT\ln J_M(N;t_1,t_2)\ . \tag{5.13}$$

$\Delta F(T,\Phi)$ contains the effect of the kinks.

The first term on the right-hand side of Eq. (5.12) must be kept if the effects of the finite size of a short chain are to be considered. However, we will be interested only in the case $M\gg1$ and thus this term will be neglected. From Eqs. (5.1) and (5.12) we calculate the value of some thermodynamic functions in the "one-well" ($F=F_0$) approximation:

$$S_0=Mk_B\left[1+\ln\left[\frac{2\pi k_BT}{(IE_2)^{1/2}}\right]-\left[\frac{(16\,|\,\eta\,|^2-1)E_1}{16\,|\,\eta\,|E_2}\right]^{1/2}+\frac{(64\,|\,\eta\,|^2-7)k_BT}{16(16\,|\,\eta\,|^2-1)E_2}\right]\ , \tag{5.14}$$

$$U_0=M\left[k_BT-(\,|\,\eta\,|+1/8\,|\,\eta\,|\,)E_1+\frac{(64\,|\,\eta\,|^2-7)(k_BT)^2}{32(16\,|\,\eta\,|^2-1)E_2}\right]\ , \tag{5.15}$$

$$C_{v0}=Mk_B\left[1+\frac{(64|\eta|^2-7)k_BT}{16(16|\eta|^2-1)E_2}\right]. \tag{5.16}$$

These results contain the phonon and lowest-order anharmonic contributions.

Let us now proceed to analyze the thermodynamic properties that depend upon the kinks, i.e., $\Delta F(T,\Phi)$ in Eq. (5.11). The number of thermally excited kinks in the sine-Gordon chain has been found to be $N(T)=M\beta|t|$, where $|t|$ is the tunneling rate. Therefore, a natural generalization permits us to express the number of thermally excited large and small kinks in the DSG chain at low temperatures as

$$N^{>}(T)=M\beta|t_2|\ , \tag{5.17a}$$

and

$$N^{<}(T)=M\beta|t_1|\ , \tag{5.17b}$$

respectively. Since $|t_2|<|t_1|$, it is clear that $N^{>}(T)<N^{<}(T)$. There will be also N large and N small kinks created by the external torque. The phase evolution corresponding to these $2N$ kinks is $\Phi=2\pi N$.

The integral in Eq. (5.10) can be carried out exactly, yielding a superposition of associated Legendre functions, but we do not find this procedure particularly illuminating. We will consider two special cases that are amenable to an easy physical interpretation.

(1) $\langle N(T)\rangle_H^{1/2}\gg N$, with $\langle N(T)\rangle_H$ denoting the harmonic mean between $N^{>}(T)$ and $N^{<}(T)$. The temperature is not too low and we have a reasonably large number of thermally excited kinks compared to the number of torque-generated kinks. A quadratic approximation for the cosine is possible and the integration can be easily performed. We obtain

$$J_M(N;t_1,t_2)=\left[\frac{(t_1+t_2)}{2\pi\beta Mt_1t_2}\right]^{1/2}\exp[\beta M(t_1+t_2)]\exp\left[-\frac{(t_1+t_2)}{2\beta Mt_1t_2}N^2\right]. \tag{5.18}$$

The contribution of this term to the free energy is, according to Eq. (5.13),

$$\Delta F(T,\Phi)=-\frac{k_BT}{2}\ln\left[\frac{k_BT}{2\pi M}\frac{(t_1+t_2)}{t_1t_2}\right]-M(t_1+t_2)+\frac{(t_1+t_2)}{2Mt_1t_2}(k_BT)^2N^2\ . \tag{5.19}$$

Thermodynamic quantities like U, S, and C_v are modified; for example, the specific heat has an extra contribution,

$$\Delta C_v(T,\Phi)=(1/2k_BT^2)\left[\frac{\langle N(T)\rangle_H}{N^{>}(T)+N^{<}(T)}(E^{>}-E^{<})^2+2(E^{>})^2N^{>}(T)\right.$$
$$\left.+2(E^{<})^2N^{<}(T)-N^2\left[\frac{(E^{>})^2}{N^{>}(T)}+\frac{(E^{<})^2}{N^{>}(T)}\right]\right]. \tag{5.20}$$

The specific heat is increased by the interaction between large and small kinks and is decreased by the interaction between topological and thermal kinks. The largest contribution to C_v is $(E^{<})^2N^{<}(T)/k_BT^2$: Small kinks are more relevant to the specific heat than large kinks.

Of particular interest is the applied torque, Eq. (4.7),

$$\tau=-(k_BT/2\pi)[N/N^{<}(T)+N/N^{>}(T)]\ . \tag{5.21}$$

The corresponding result in the sine-Gordon problem is[2] $\tau=-k_BTN/2\pi N(T)$: For a fixed phase evolution $2\pi N$, the torque required to support that phase evolution is proportional to $1/N(T)$; the more thermal kinks the chain has, the easier it is to generate phase. According to Eq. (5.21), the increase in the number of one type of kink in the DSG chain facilitates the phase evolution over the corresponding barrier. Since $N^{<}(T)>N^{>}(T)$, and often $N^{<}(T)\gg N^{>}(T)$, the torque required to provide a given phase evolution is determined by the number of thermally excited large kinks.

We can also compute the average phase displacements. From Eq. (4.18),

$$f_{\mu\nu}=(1/2\pi)\sum_l e^{2\pi il(\nu-\mu)}f(l,l)\ , \tag{5.22}$$

where $f(l,l)=(2\pi)^2 l$ if $f(\theta)=\theta$ and $f(l,l)=(2\pi)^3 l^2$ if $f(\theta)=\theta^2$ and we consider only the most important term. Setting Eqs. (5.8), (5.10), and (5.22) into (4.17) we easily get

$$\langle f(\theta_{n+1})\rangle=\frac{1}{(2\pi)}\sum_l f(l,l)\frac{J_{M-n}(N-l;t_1,t_2)J_n(l;t_1,t_2)}{J_M(N;t_1,t_2)} . \tag{5.23}$$

This expression can be evaluated in the quadratic limit with the help of Eq. (5.18),

$$f(\theta_{n+1})=\left[\frac{(t_1+t_2)M}{8\pi^3\beta t_1 t_2(M-n)}\right]^{1/2}\sum_l f(l,l)\exp\left[-\frac{(t_1+t_2)M}{2\beta t_1 t_2 n(M-n)}\left[\frac{Nn}{M}-l\right]^2\right] . \tag{5.24}$$

If $\langle N(T)\rangle_H \gg 1$, the sum can be replaced by an integral whose evaluation is straightforward. We obtain

$$\langle\theta_{n+1}\rangle=2\pi N\left[\frac{n}{M}\right]\equiv x_n\Phi , \tag{5.25}$$

$$\langle\theta_{n+1}^2\rangle=x_n^2\Phi^2+(2\pi)^2 x_n(1-x_n)\langle N(T)\rangle_H . \tag{5.26}$$

Hence, the variance corresponding to the phase of the $(n+1)$th particle is

$$\langle\theta_{n+1}^2\rangle-\langle\theta_{n+1}\rangle^2=(2\pi)^2 x_n(1-x_n)\langle N(T)\rangle_H . \tag{5.27}$$

In this regime, the fluctuations in the phase are controlled by the harmonic mean number of thermally excited kinks. (See Fig. 7.) If $N^>(T) \ll N^<(T)$, $\langle N(T)\rangle_H \approx N^>(T)$, the number of greater kinks determines the size of the fluctuations.

(2) $t_2 \ll t_1$. The tunneling rates through both barriers are very different and Eq. (5.10) can be approximately written as

$$J_M(N;t_1,t_2)=(1/2\pi)e^{M\beta t_1}\int_{-\pi}^{\pi} e^{-iNx}e^{M\beta t_2\cos x}dx$$
$$=e^{M\beta t_1}T_N(M\beta t_Z) , \tag{5.28}$$

where I_N is a Bessel function. (See Fig. 8.) The only contribution to the band structure comes from the tunneling through the larger barriers, the tunneling through the smaller ones manifesting itself only through the splitting of the ground-state energy level. Therefore, except for the factor $e^{M\beta t_1}$ accounting for this splitting, our problem has been reduced to that of a sine-Gordon chain characterized by a tunneling rate t_2. The properties of such a system have been treated in detail in Ref. 2. The correction to the free energy due to collective effects is

$$\Delta F(T,\Phi)=-Mt_1-k_B T\ln I_N(M\beta t_2) . \tag{5.29}$$

The average values can be obtained setting Eq. (5.28) into (5.23),

$$\langle f(\theta_{n+1})\rangle=\frac{1}{2\pi}\sum_l f(l,l)\frac{I_{N-l}((M-n)\beta t_2)I_l(n\beta t_2)}{I_N(M\beta t_2)} . \tag{5.30}$$

In the limits $N\gg N^>(T)$, $N\ll N^>(T)$, we can obtain explicit results for the torque and the position fluctuations,

$$\tau=\begin{cases}\dfrac{k_B T}{2\pi}\left[\ln\dfrac{N^>(T)}{2N}-\dfrac{1}{2N}+\cdots\right], & N\gg N^>(T)\\ -\dfrac{k_B T}{2\pi}\dfrac{N}{N^>(T)}, & N\ll N^>(T) ,\end{cases} \tag{5.31}$$

$$\langle\theta_{n+1}^2\rangle-\langle\theta_{n+1}\rangle^2=\begin{cases}x_n(1-x_n)(2\pi)^2 N , & N\gg N^>(T)\\ x_n(1-x_n)(2\pi)^2 N^>(T) , & N\ll N^>(T) .\end{cases} \tag{5.32}$$

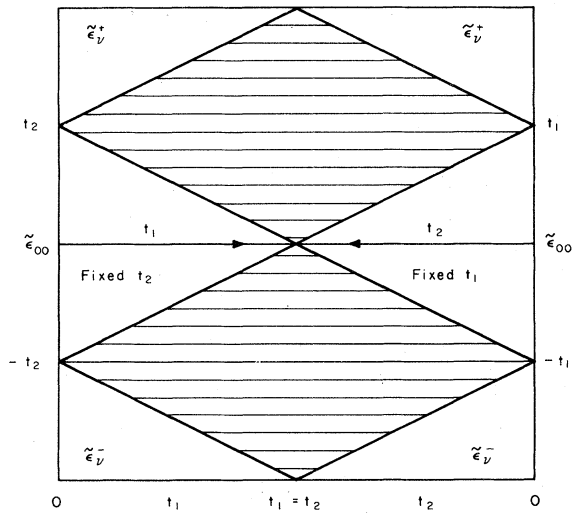

FIG. 8. Band structure. The tight-binding bands are shown as functions of the tunneling rates. If $t_1=t_2$ there is only one band, meaning that all the sites are equivalent, while if either t_1 or t_2 vanishes we get the splitting corresponding to an isolated two-well system.

From Eqs. (5.31) and (5.32) we can see that in the case $t_2 \ll t_1$ the small kinks do not have any effect whatsoever on the collective properties of the chain. There may be many thermally excited smaller kinks but the topology of the system does not allow them to contribute to the size of the fluctuations.

We can now discuss qualitatively the expected behavior of the system and the influence of temperature. At $T=0$ K we have a kink lattice [Fig. 9(a)] in which small and large kinks alternate. It is clear that small and large kinks of the same sign must repel each other in order to minimize the elastic energy. At $T=0^+$, thermal fluctuations cause the kink lattice to melt, and the kinks abandon their lattice positions, moving along the chain; of course, their motion is limited by the topological constraints imposed by the potential. At $T>0$ K thermal kinks and antikinks appear, the number of small kinks being larger than the number of large kinks; if the tunneling rates are very different, $N^>(T) \ll N^<(T)$, and at sufficiently low temperatures the chain will have the appearance shown in Fig. 9(b). At higher temperatures the departure of a given pendulum from its mean position $x_n\Phi$ is characterized by the mean number of thermal kinks, $\langle N(T)\rangle_H^{1/2}$, through the random-walk-like equation (5.27). If the tunneling rates are very different, the size of these fluctuations is determined solely by the number of thermally excited large kinks. At even higher temperatures the kink picture loses its meaning and the size of the fluctuations, being of the order of $M^{1/2}$, is determined by the total number of pendula in the system.

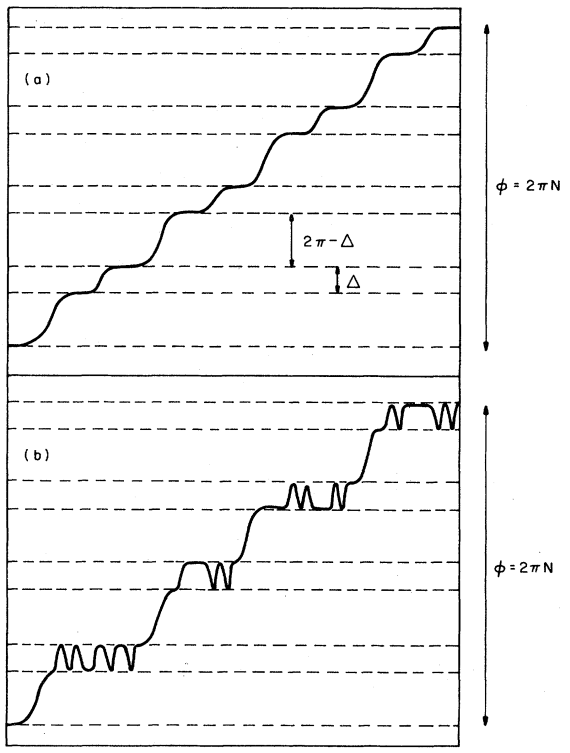

FIG. 9. Phase evolution: $\eta < -0.25$. There is an external torque causing a total phase evolution $\Phi=2\pi N$. Each one of the small kinks generates a phase evolution $\Delta=2\cos^{-1}(\frac{1}{4}|\eta|)$, while each of the large kinks yields a phase evolution equation to $2\pi-\Delta$. We show in (a) the kink lattice occurring at $T=0$ K, and in (b) the kink system at $T>0$ K in the case $t_1 \gg t_2$, when $N^<(T)$ can become large while $N^>(T)$ is essentially zero. The melting of the kink lattice implies that the large kinks will not necessarily be at their "official" positions. The dashed lines mark the position of the degenerate minima.

B. $\eta > -\frac{1}{4}$

The potential has the shape described in Figs. 1 and 4 if $|\eta| < \frac{1}{4}$ and in Figs. 1 and 5 if $\eta > \frac{1}{4}$. In both cases, however, there is only one kind of true vacuum per unit cell. The ground-state energy level associated with one of these vacua can be obtained using the same approximation that led to Eq. (5.1). We now have

$$\beta\tilde{\epsilon}_{00}=-\lambda_1\{1+\eta-[(1+4\eta)/4\lambda_1\lambda_2]^{1/2}+(1+16\eta)/32(1+4\eta)\lambda_1\lambda_2\}\ . \tag{5.33}$$

The tight-binding band corresponding to these ground-state energies has the conventional shape described by Eq. (A10). We write

$$\tilde{\epsilon}_v=\tilde{\epsilon}_{00}-t\cos 2\pi\nu\ , \tag{5.34}$$

where t is the tunneling rate, which can be calculated again in the WKB approximation using Eqs. (5.3) and (5.4); the harmonic-oscillator ground-state energy is

$$\beta E(T)=[(1+4\eta)/4]^{1/2}(\lambda_1/\lambda_2)^{1/2}\ . \tag{5.35}$$

A simple calculation shows that the exponential in the tunneling rate is again proportional to the kink energy $P=\beta E_\phi^>$.

Using the tight-binding wave function,

$$\psi_\nu(\theta)=(2\pi)^{1/2}\sum_j e^{i2\pi\nu j}\chi_0(\theta-2\pi j)\ , \tag{5.36}$$

the partition function is computed to yield

$$Z=(2\pi k_BT/I)^{(M-1)/2}[\lambda_1\lambda_2(1+4\eta)/\pi^2]^{1/4}\times e^{-(M/2)\ln(\lambda_2/2\pi)}e^{-M\beta\tilde{\epsilon}_{00}}I_N(M\beta t)\ . \tag{5.37}$$

The argument of the Bessel function is again to be interpreted as the number of thermally excited kinks in the system.

The free energy can be obtained as the sum of

$$F_0(T,0)=\frac{k_BT}{4}\ln\left[\frac{4(\pi k_BT)^4}{I^2(1+4\eta)E_1E_2}\right]-k_BTM\ln\left[\frac{2\pi k_BT}{(IE_2)^{1/2}}\right]+M\tilde{\epsilon}_{00} \tag{5.38}$$

and

$$\Delta F(T,\Phi)=-k_BT\ln I_N(M\beta t)\ . \tag{5.39}$$

If $M\gg 1$ we get the following values for the thermodynamic functions in the lowest order:

$$S_0=Mk_B\left[1+\ln\left[\frac{2\pi k_BT}{(IE_2)^{1/2}}\right]-\left[\frac{1+4\eta}{4}\right]^{1/2}\left[\frac{E_1}{E_2}\right]^{1/2}+\frac{1+16\eta}{16(1+4\eta)}\frac{k_BT}{E_2}\right]\ , \tag{5.40}$$

$$U_0=M\left[k_BT-E_1(1+\eta)+\frac{1+16\eta}{32(1+4\eta)}\frac{(k_BT)^2}{E_2}\right]\ , \tag{5.41}$$

$$C_{v0}=Mk_B\left[1+\frac{(1+16\eta)}{16(1+4\eta)}\frac{k_BT}{E_2}\right]\ . \tag{5.42}$$

The collective properties, torque, and phase fluctuations are formally analogous to those corresponding to the sine-Gordon problem and are represented by the results in Eqs. (5.31) and (5.32), with the condition $N\gg(\ll)\ N^>(T)$ replaced by $N\gg(\ll)\ N(T)=M\beta t$.

VI. DYNAMICS

In this section, we examine the DSG chain in an external field; each paritcle is subject to a uniform external torque. Because the ends of the chain are free and thus the torque produces a nonzero phase evolution of the entire chain, i.e., a current, we are dealing with a nonequilibrium situation. This problem, when studied in detail[3,13,18] for the usual SG chain, yielded the following picture for the phase-current versus external-field characteristics. At low fields and low temperatures, the phase evolved by a mechanism which could be identified as the motion of kinks that are produced by thermal fluctuations. As the external field is increased and reaches the same order of magnitude as the barrier height of the SG potential [E_1 in Eq. (3.1)], nonlinear evolution is found[19] where the current can increase by decades due to a small increase in the external field. Finally, for large external fields and/or high temperatures, the barrier to phase evolution is completely degraded and the current is simply proportional to the applied field, Ohm's law.

It is clear that going from the SG to the DSG potential is not going to affect the behavior of the current at high fields and temperatures. In the other extreme, however, we might expect some novel behavior because of the presence of extra structure in the periodic potential and the possibility of an additional kink. In the following, we outline briefly our method of calculation (for the details the reader is directed to Refs. 3 and 18) and then discuss those new features in the behavior of the system that are due to the modified potential.

We consider a discretized chain with M sites whose Hamiltonian is written, Eq. (3.1),

$$H=\sum_{i=1}^{M}\left[\tfrac{1}{2}I\dot{\theta}_i^2-E_1(\cos\theta_i+\eta\cos 2\theta_i)\right.$$
$$\left.+\tfrac{1}{2}E_2(\theta_{i+1}-\theta_i)^2\right] . \quad (6.1)$$

The finite-temperature nonequilibrium behavior of the chain is described by a Fokker-Planck equation together with the Langevin equation associated with the equations of motion derived from Eq. (6.1).[3,18] In the overdamped limit, the Fokker-Planck equation describes a diffusive motion through configuration space,

$$\frac{\partial\sigma_M}{\partial t}+\vec{\nabla}_M\cdot\vec{J}_M=0 , \quad (6.2)$$

where σ_M is the M-particle configuration-space distribution function and the ith component of the current $\vec{J}_M$ can be written

$$J_M^{(i)}=-\frac{1}{\tau}e^{-\beta U}\frac{\partial}{\partial i}(e^{\beta U}\sigma_M) . \quad (6.3)$$

In the above,

$$\frac{\partial}{\partial i}=\frac{\partial}{\partial\theta_i} ,$$

$\tau\equiv\beta I\gamma$, where γ is a phenomenological damping, and

$$U\equiv V+V_{\text{ext}} , \quad (6.4)$$

where V is the potential-energy function in the Hamiltonian, Eq. (6.1), and V_{ext} is the applied torque which we take to be of the form

$$V_{\text{ext}}=-E_0\sum_{i=1}^{M}\theta_i . \quad (6.5)$$

Equation (6.2) is known as the Smolouchowski equation (SE). In the following we shall look for a *steady-state* solution to the SE. To this end we write

$$\sigma_M\equiv e^{-\beta V+w_M} , \quad (6.6)$$

which defines the quantity w_M. Using (6.6), the probability current becomes

$$J_M^{(i)}=-\frac{1}{\tau}\sigma_M\frac{\partial}{\partial i}(w_M+\beta V_{\text{ext}}) . \quad (6.7)$$

One may generate from the SE

$$\sum_i\frac{\partial}{\partial i}J_M^{(i)}=0 ,$$

a sequence of reduced SE's by integrating out increasing numbers of site variables. In particular, by integrating out $M-1$ coordinates, we obtain the lowest-order SE,

$$\frac{\partial}{\partial 1}J_1(1)=0 , \quad (6.8)$$

where J_1 is a one-particle current. Thus J_1 is a constant current which we denote by $\overline{W}$. Solution for $\overline{W}$ can be self-consistently enforced upon assuming a single-particle form for the function w_M,

$$w_M=\sum_{i=1}^{M}w(i) . \quad (6.9)$$

Then from Eq. (6.7) we obtain

$$\left[\frac{\partial w(1)}{\partial 1}-\lambda_0\right]\sigma_1(1)=-\overline{W}\tau , \quad (6.10)$$

where

$$\lambda_0\equiv\beta E_0 , \quad (6.11)$$

and

$$\sigma_1(1)=\int_{-\infty}^{\infty}d2\cdots dM\,\sigma_M(1,\ldots,M) \quad (6.12)$$

is the single-particle nonequilibrium distribution function, which itself depends on $w(1)$ through Eq. (6.6). By requiring that $w(\theta)=w(\theta\pm 2\pi m)$, with m an integer (which follows from the periodicity of σ_M in the steady state), we obtain from Eq. (6.10)

$$\overline{W}\tau=\frac{2\pi\lambda_0}{\int_0^{\pi}\frac{d\theta}{\sigma_1(\theta)}} . \quad (6.13)$$

Equations (6.10), (6.12), and (6.13) can now be solved self-consistently for $\overline{W}$ and $w(\theta)$ for a given set of potential parameters, external field, and viscous damping. Equation (6.12) is solved by a transfer-integral technique which uses the normalization

$$\int_0^{2\pi}\sigma_1(\theta)d\theta=1 . \quad (6.14)$$

We note that the high-field, and/or high-temperature asymptotic behavior discussed above can be immediately read from Eq. (6.13). In these limits $\sigma_1\sim$const, which can be obtained from the normalization, Eq. (6.14); thus

$$\frac{\overline{W}\tau}{\beta}\sim\frac{E_0}{2\pi} . \quad (6.15)$$

The participation of kinks in the current can also be inferred from Eq. (6.13) since it is the *minimum* value of $\sigma(\theta)$ which determines the magnitude of the current. At low temperatures and small fields a

strong minimum occurs at $\theta \approx \pi$. We thus have

$$\overline{W}\tau \approx 2\pi\lambda_0\sigma(\pi) . \tag{6.16}$$

The value $\sigma(\pi)$ is related to the probability that a particle is on the barrier,[3] i.e., at π. This probability is proportional to the number of kinks for it is the kinks that carry particles onto the barrier.

A. The current

Let us examine the effects of the potential parameter η on the characteristics of the system. In the following, we use a system of reduced units whereby energies are measured in units of the $\eta=0$ barrier height E_1. These reduced quantities will usually be denoted by an asterisk (viz., $\beta^* \equiv \beta E_1$, $\alpha \equiv E_0/E_1$, $V^* = V/E_1$, etc.) and in particular, from Eq. (5.11), $\lambda_0 = \beta^*\alpha$. All results to be reported in this section will be for coupling strength $\xi^2 \equiv E_2/E_1 = 1.0$.

In Table I we show the current $\overline{W}$ as a function of η at the temperatures $\beta^*=2.0$ and 4.0. There is a maximum in $\overline{W}$, at $\eta \sim -0.8$, for both temperatures. [It is clear that there must be a maximum somewhere since $\overline{W}$ is (presumably) continuous in η, positive, and vanishes as $\eta \to \pm\infty$.] The reason why the maximum in fact occurs at negative rather than positive η can be inferred from Fig. 10. There we have sketched $V^*(\theta)$ and $\sigma(\theta)$ at $\beta^*=4.0$ for $\eta = \pm 0.4$. In terms of a kink-conduction process, the much smaller current for the $\eta=0.4$ potential (cf. Table I) is a consequence of the much wider "barrier region". It is much more difficult to create a kink for $\eta=+0.4$ than it is for $\eta=-0.4$. Of course the current cannot increase indefinitely as η is made more negative since the increase in barrier *height* will eventually dominate and as $|\eta| \to +\infty$ the current goes to zero as $\exp(-A\sqrt{\eta})$.

TABLE I. The dependence of the phase current $\overline{W}$ and the activation energy E_a^* on the parameter η. (The external field $\alpha = 10^{-4}$.)

	$\frac{\overline{W}\tau}{\beta}$		
η	$\beta^*=2.0$	$\beta^*=4.0$	E_a^*
1.00	1.5×10^{-11}	8.0×10^{-20}	10.1
0.80	2.6×10^{-11}	2.1×10^{-19}	9.8
0.60	4.9×10^{-11}	2.3×10^{-18}	9.6
0.40	1.1×10^{-10}	4.3×10^{-18}	9.0
0.25	2.1×10^{-10}	2.2×10^{-17}	8.5
0.10	4.6×10^{-10}	7.5×10^{-17}	8.1
0.0	8.0×10^{-10}	3.2×10^{-16}	7.6
−0.10	1.4×10^{-9}	1.6×10^{-15}	7.1
−0.25	3.5×10^{-9}	2.2×10^{-14}	6.0
−0.40	8.0×10^{-9}	3.2×10^{-13}	
−0.60	1.8×10^{-8}	1.6×10^{-12}	6.3
−0.80	2.3×10^{-8}	1.1×10^{-12}	6.7
−1.00	1.8×10^{-8}	2.2×10^{-13}	7.0

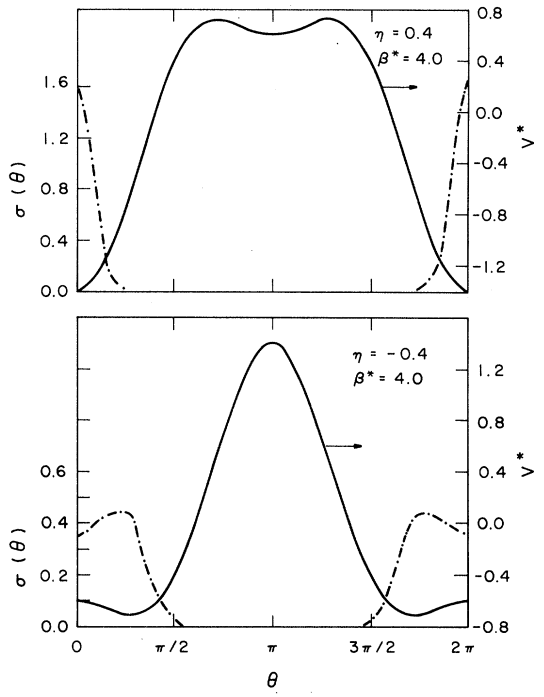

FIG. 10 $V^*(\theta)$ and $\sigma(\theta)$. The single-particle potential $V^*(\theta)$ and the single-particle density $\sigma(\theta)$ are plotted vs θ for $\eta=+0.4$, $\beta^*=4.0$, and $\eta=-0.4$, $\beta^*=4.0$. The single-particle potential strongly influences the structure and energy of a kink, the single-particle density, etc.

In Fig. 11 (and Table I) we show the results of an activation-energy E_a^* analysis of the current. The values of E_a^* plotted in this figure are found from the slope of a plot of $\ln(\overline{W}\tau)$ vs β^*. The solid line in Fig. 11 is the energy of the large kink $E_\phi^>(\eta)^*$, calculated in the continuum approximation; see the equations in Sec. II. The good qualitative agreement between the η dependence of E_a^* and the η dependence of the kink energies $E_\phi^{>*}$ support the point of view that the low-temperature, low-field current is carried by thermally activated kinks. We note that the best agreement between E_a^* and $E_\phi^{>*}$ occurs for small values of η. As $|\eta|$ increases the agreement tends to become worse; however, we can make no absolute statements as to whether the cause of the disagreement is physics (i.e., discrete versus continuum systems) or numerics. (For positive η, the activated region usually began for $\beta^* \gtrsim 4.0$ and the numerical work tended to become unreliable for $\beta^* > 10.0$ [because of the strongly

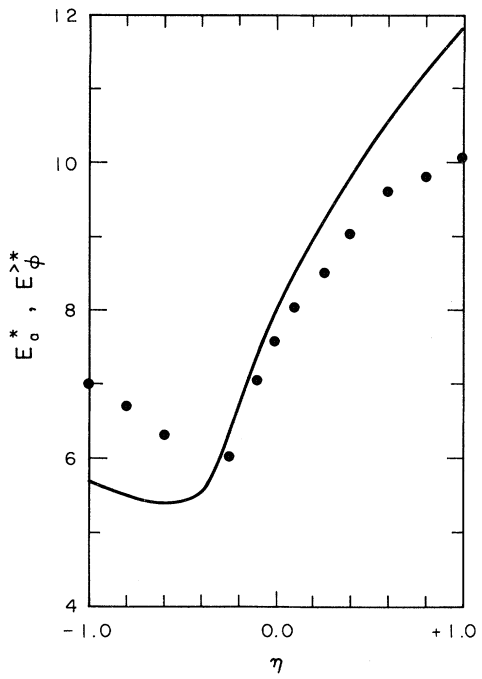

FIG. 11. Energies. The energy E_a^*, taken from analysis of the temperature dependence of the current at fixed η, is plotted as a function of η. Shown also is E_ϕ^* (continuous line) from the analytic determination of the kink energy described in Sec. II.

peaked nature of $1/\sigma(\theta)$]. For negative η (<-0.25) the situation is somewhat more complicated as will be discussed below.)

One striking aspect of Fig. 11 is the abrupt change in the relationship of E_ϕ^* to E_a^* as η is decreased below -0.25. As discussed in the previous section, in this region of η the potential develops a two-well structure symmetrically located about $\theta=0$ (cf. Fig. 10). One feature of this potential is the possibility of the creation of a second ("small") kink. We find no direct evidence for the participation of the small kink in the current-carrying process. That is, the current is dominated by thermal activation over the higher barrier. (To be more precise, we can say that for $\eta=-1.0$, for example, the log of the current is linear in β^* for $4<\beta^*<10$ and shows no evidence of two-exponential activation as might be expected from a phenomenological kink-gas picture.[17]

B. Polarization

In our calculation, the important consequence of the two-well structure is the appearance of a strong polarization[20] phenomenon which is the precursor to activation.

In Fig. 12 we plot $\ln(\overline{W}\tau/\alpha)$ and $\ln\langle\theta\rangle$ vs β^* for $\eta=-0.6$ at the two field strengths $\alpha=10^{-3}$ and 10^{-5}. If we first examine the current, we note that at high temperatures the curves coincide and as β^* is increased past ~ 4.0 they separate. This remarkable behavior is unlike anything seen in the ordinary sine-Gordon problem. In the SG system, we argued that for small α we could simply replace $\sigma(\theta)$ by $\rho(0)$ (the equilibrium-distribution function) and thus $\overline{W}\tau$ would be determined by linear response. That is, $\overline{W}\tau/\alpha$ should be independent of α for small α [cf. Eq. (6.13), $\lambda_0\equiv\beta^*\alpha$]. Figure 12 shows that this linear-response description is not appropriate to the DSG chain (with $\eta<-0.25$) if the temperature is made low enough. The reason for this behavior can be understood by now examining $\langle\theta\rangle$ as a function of β^*. As the temperature is lowered, the system becomes polarized (i.e., $\langle\theta\rangle\neq 0$) because of the external field. The degree of polarization (at a given β^*) depends on the magnitude of the field. Thus in Fig. 12 we see that the system with $\alpha=10^{-3}$ is strongly polarized by $\beta^*\sim 5.0$ whereas for $\alpha=10^{-5}$ the system is still not strongly polarized at $\beta^*=7.0$ (at $\beta^*=\infty$ the system will be found at $\langle\theta\rangle=1.141$). The trend toward strong polarization in the $\alpha=10^{-3}$ system is vividly shown in Fig. 13 where $\sigma(\theta)$ is plotted for $\beta^*=2.0$, 4.0, 6.0, and 8.0. In summary then, we find that the low-field,

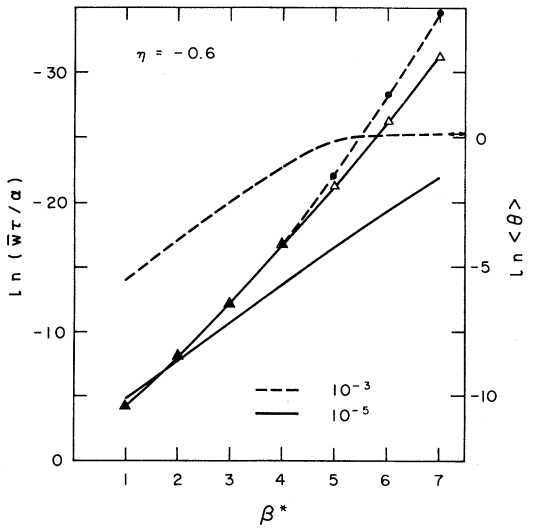

FIG. 12. Current and polarization. Two measures of the chain response to an external field, the current $\overline{W}$, and the polarization $\langle\theta\rangle$, are plotted vs β^*, T^{-1}, for two different values of the field. The current is a weak function of the field; the polarization, involving the small kink, is a strong function of the field.

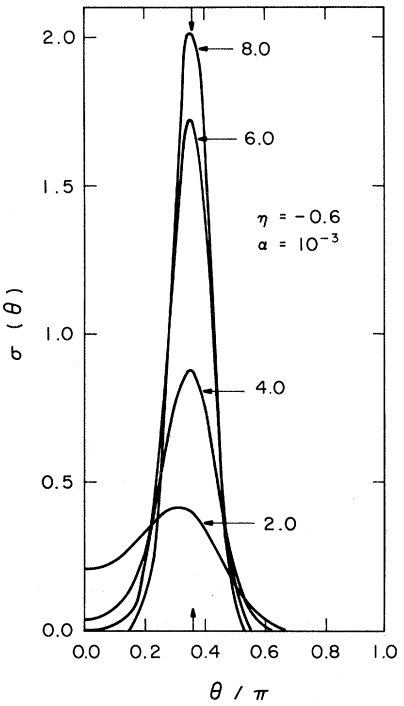

FIG. 13. Single-particle density. The single-particle density $\sigma(1)$ is plotted vs θ for fixed α and η. As the temperature becomes lower, β^* goes from 2 to 8, and the particles become more and more polarized.

low-temperature current in the DSG chain (with $\eta < 0.25$) is *nonlinear* in the external field. In addition, the current is activated only *after* the system has polarized (cf. Fig. 12). It is this after-polarization activation energy which is plotted in Fig. 11. (We note that in Table I there is no entry for E_a^* at $\eta = -0.4$. This is because of the very weak double-well structure. The temperatures at which the system is strongly polarized are below those we could reach maintaining confidence in the numerical work.)

We shall end this section by discussing the nature of the strongly polarized state. At $\beta^* = \infty$, the particles on the chain will be δ function localized at $\Theta = \cos^{-1}(1/4\eta)$, the position of the minimum in the potential. As the temperature is raised the single-particle density acquires a width and the particles sense the large barrier at $\theta = \pi$ and the small barrier at $\theta = 0$. Eventually, a high-enough temperature is reached such that thermal fluctuations will activate large sections of chain over the (small) barrier. In the language of nucleation theory,[13] when these sections become larger on the average than a critical size (the critical nucleus) a stable small kink-antikink pair will be produced, whose manifestation will be an increased probability of finding the system at $\theta = -\Theta$ (i.e., decreased polarization). That is, *depolarization is an activation process.* If we examine the $\ln\langle\theta\rangle$ vs β^* curves (for $\eta = -0.6$) in Fig. 12 we see that, indeed, in the temperature region where the system is delocalized out of the well ($\beta^* < 4.0$), $\ln\langle\theta\rangle$ is *linear* in β^*. In Fig. 14 we have plotted the activation energy obtained from $\ln\langle\theta\rangle$ vs β^* plots, at $\eta = -0.6$, -0.8, and -1.0, together with the energy of the continuum small kink. The agreement between the two is excellent. In further support of the activation picture, we also show in Fig. 14 the results of an activation-energy analysis for a system with $\eta = -0.6$ but $\xi^2 \equiv E_2/E_1 = 2.0$. From Sec. II we see that the small-kink energy is proportional to ξ. The ratio of the activation energy for the $\xi^2 = 2.0$ and $\xi^2 = 1.0$ systems is almost exactly $\sqrt{2}$. The polarization phenomena involving the small kinks can be modeled quantitatively with a suitably parametrized Ising model.

VII. CONCLUSION

We have examined the thermodynamic properties of the DSG chain both analytically and numerically. In the regime in which both small and large kinks occur on the chain we find that the importance of one or the other of these kinks depends upon the property being investigated. The small kinks dominate many thermal properties, e.g., entropy, specific heat, etc. The large kinks are involved in properties that are sensitive to phase evolution, e.g., fluctuation in the phase along the chain,

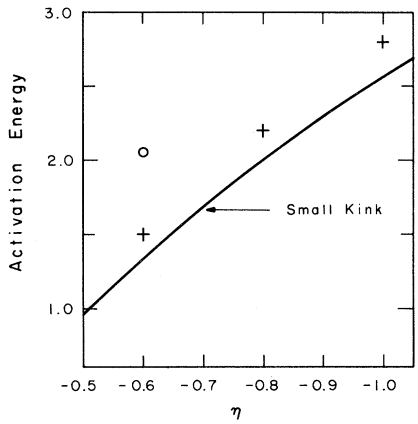

FIG. 14. Polarization and activation. From an analysis of $\langle\theta\rangle$ vs β^*, e.g., Fig. 12, the polarization is found to involve thermal activation of small kinks. The activation energy, from an analysis of $\langle\theta\rangle$ vs β^*, is plotted vs η.

the equation of state, and the phase current. The small kinks are also seen in a polarization phenomena that is a precursor to thermally activated large-kink conductivity.

ACKNOWLEDGMENT

This work was supported in part by the National Science Foundation.

APPENDIX A: THE TIGHT-BINDING BANDS

If $\eta < -0.25$, the DSG system can be suitably described, in the case $1 \ll \lambda_1 \ll \lambda_2$, by the tight-binding Hamiltonian

$$H_{TB} = \sum_j [\tilde{\epsilon}_{00}(C_{Lj}^\dagger C_{Lj} + C_{Rj}^\dagger C_{Rj}) + t_1(C_{Rj}^\dagger C_{Lj} + C_{Lj}^\dagger C_{Rj}) + (t_2/2)(C_{Rj}^\dagger C_{Lj+1} + C_{Lj}^\dagger C_{Rj+1} + C_{Lj+1}^\dagger C_{Rj} + C_{Rj+1}^\dagger C_{Lj})] , \quad \text{(A1)}$$

where $\tilde{\epsilon}_{00}$ is the lowest energy level in each individual well, t_1 and t_2 represent the tunneling rates through the lower and higher barriers, respectively, and $C_{Rj}^\dagger(C_{Rj})$ and $C_{Lj}^\dagger(C_{Lj})$ are the creation (destruction) operators for particles in the right- and left-hand wells of the jth cell. (See Fig. 15.) Defining the new operators $C_{Rv}^\dagger, \ldots$, through

$$C_{Rj}^\dagger = \sum_\nu e^{i2\pi j\nu} C_{R\nu}^+ \quad \text{(A2a)}$$

and

$$C_{Lj}^\dagger = \sum_\nu e^{i2\pi j\nu} C_{L\nu}^\dagger , \quad \text{(A2b)}$$

we can write Eq. (A1) as a sum over ν:

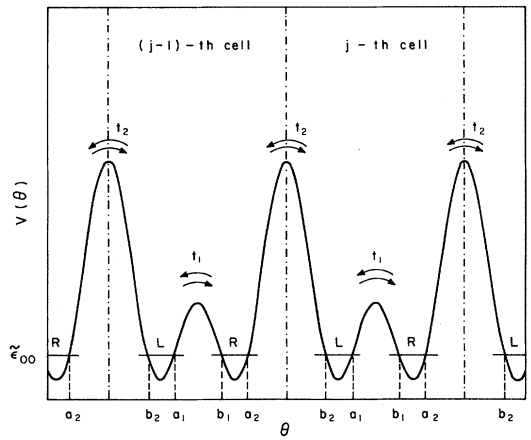

FIG. 15. Tunneling rates. In region I there are two kinds of kinks. Their appearance in the thermodynamics comes from consideration of the tunneling processes in the potential $V(\theta)$. Each repeating cell contains a left-hand well (L) and a right-hand well (R). The single-well energy levels $\tilde{\epsilon}_{00}$ and the two types of tunneling rates, labeled t_1 and t_2, are indicated.

$H_{TB} = \sum_\nu H_\nu$, with

$$H_\nu = \tilde{\epsilon}_{00}(C_{L\nu}^\dagger C_{L\nu} + C_{R\nu}^\dagger C_{R\nu}) + t_1(C_{R\nu}^\dagger C_{L\nu} + C_{L\nu}^\dagger C_{R\nu}) + t_2(e^{-i2\pi\nu} C_{R\nu}^\dagger C_{L\nu} + e^{+i2\pi\nu} C_{L\nu}^\dagger C_{R\nu}) . \quad \text{(A3)}$$

This Hamiltonian can be diagonalized in terms of the operators $\alpha_\nu^\dagger$ and α_ν, where

$$\alpha_\nu^\dagger = u_\nu C_{L\nu}^\dagger + v_\nu C_{R\nu}^\dagger . \quad \text{(A4)}$$

The diagonal form is obtained by requiring that $\alpha_\nu^\dagger$ satisfies the condition

$$[\alpha_\nu^\dagger, H_\nu] = -\tilde{\epsilon}_\nu \alpha_\nu^\dagger . \quad \text{(A5)}$$

On the other hand, if we employ Eqs. (A3) and (A4) to compute the commutator explicitly, we get

$$[\alpha_\nu^\dagger, H_\nu] = -[u_\nu \tilde{\epsilon}_{00} + v_\nu(t_1 + t_2 e^{i2\pi\nu})] C_{L\nu}^\dagger - [v_\nu \tilde{\epsilon}_{00} + u_\nu(t_1 + t_2 e^{-i2\pi\nu})] C_{R\nu}^\dagger . \quad \text{(A6)}$$

Comparing the right-hand sides of Eqs. (A5) and (A6), we get the pair of equations,

$$(\tilde{\epsilon}_{00} - \tilde{\epsilon}_\nu) u_\nu + (t_1 + t_2 e^{+i2\pi\nu}) v_\nu = 0 , \quad \text{(A7a)}$$

and

$$(t_1 + t_2 e^{-i2\pi\nu}) u_\nu + (\tilde{\epsilon}_{00} - \tilde{\epsilon}_\nu) v_\nu = 0 . \quad \text{(A7b)}$$

The compatibility condition for these two equations yields

$$\tilde{\epsilon}_\nu^\pm = \tilde{\epsilon}_{00} \pm (t_1^2 + t_2^2 + 2t_1 t_2 \cos 2\pi\nu)^{1/2} . \quad \text{(A8)}$$

This is the equation describing the tight-binding energy bands. Note that it is symmetric in t_1 and

t_2, as it should be. An important special case of Eq. (A8) occurs when one of the tunneling rates is much larger than the other, e.g., $t_2 \ll t_1$. Then

$$\tilde{\epsilon}_\nu^{\pm} = \tilde{\epsilon}_{00} \pm (t_1 + t_2 \cos 2\pi\nu) \ . \tag{A9}$$

The lowest barrier splits the ground state while the highest barrier provides the band structure. If the height of the barrier characterized by t_1 tends to zero, we will have a single well per unit cell, and the energy $\tilde{\epsilon}_\nu^-$ in Eq. (A9) can be conveniently rewritten as

$$\tilde{\epsilon}_\nu^- = \tilde{\epsilon}'_{00} - t_2 \cos 2\pi\nu \ , \tag{A10}$$

where $\tilde{\epsilon}'_{00} = \tilde{\epsilon}_{00} - t_1$ determines the true position of the ground-state energy corresponding to the isolated single well. Equation (A10) is the usual tight-binding result for a system having only one well per unit cell, as it occurs with the DSG chain when $\eta > -0.25$.

If we let $t_2 \to 0$ in Eq. (A9), then $\tilde{\epsilon}_\nu^{\pm} \to \tilde{\epsilon}_{00} \pm t_1$: The band structure disappears and we get the level splitting corresponding to an isolated double well.

APPENDIX B: THE TRANSFER INTEGRAL AT LOW TEMPERATURE

As $T \to 0$ K, both λ_1 and λ_2 are large compared to one and some meaningful results can be obtained directly from the transfer integral. We deal separately with the cases $\eta > -\frac{1}{4}$ and $\eta < -1/4$.

A. $\eta > -\frac{1}{4}$

There is only one minimum per unit cell, and the solution to Eq. (4.20) can be taken to be

$$\psi_\nu(\theta) = \frac{1}{\sqrt{2\pi}} \sum_j e^{2\pi\nu j i} \chi_0(\theta - 2\pi j) \ , \tag{B1}$$

with $\chi_0(\theta - 2\pi j)$ solving approximately the transfer-integral problem near $\theta = 2\pi j$. Assuming $\chi_0(\theta - 2\pi j)$ is a Gaussian centered at $\theta = 2\pi j$,

$$\chi_0(\theta - 2\pi j) = A \exp[-(\alpha^2/2)(\theta - 2\pi j)^2] \ , \tag{B2}$$

we can integrate over θ_2 in Eq. (4.20) to obtain

$$\alpha^2(\eta) = (1+4\eta)^{1/2}(\lambda_1\lambda_2)^{1/2} \times [1 + \tfrac{1}{2}(1+4\eta)^{1/2}(\lambda_1/\lambda_2)^{1/2} + O(\lambda_1/\lambda_2)] \tag{B3}$$

and

$$\beta\epsilon_0(\eta) = -\lambda_1(1+\eta) - \tfrac{1}{2}\ln(2\pi/\lambda_2) + \tfrac{1}{2}(1+4\eta)^{1/2}(\lambda_1/\lambda_2)^{1/2} + O(\lambda_1/\lambda_2) \ . \tag{B4}$$

This result agrees with the one obtained in the parabolic approximation to the differential form of the transfer problem. [See Eq. (5.33)].

The normalization condition yields

$$|\chi(0)|^2 = 2\pi^{1/2}[\lambda_1\lambda_2(1+4\eta)]^{1/4} e^{\lambda_1(1+4\eta)} \ . \tag{B5}$$

B. $\eta < \frac{1}{4}$

There are two minima per unit cell, located at $\theta = 2n\pi \pm \Theta$, for all integers n. Here

$$\Theta = |\cos^{-1}(\tfrac{1}{4}|\eta|)| \ .$$

Owing to the similar shape of the potential near both minima, the solution to Eq. (4.20) appropriate to low temperatures can be written in the form

$$\psi_\nu(\theta) = \frac{1}{\sqrt{2\pi}} \sum_j e^{2\pi\nu j i}[\chi_0(\theta - 2\pi j - \Theta) + \chi_0(\theta - 2\pi j + \Theta)] \ , \tag{B6}$$

with χ_0 having again the form specified into (B2). Substitution into Eq. (4.20) and integration over θ_2 yields

$$\alpha^2(\eta) = 2(|\eta| - 1/16|\eta|)^{1/2}[1 + (|\eta| - 1/16|\eta|)(\lambda_1/\lambda_2)^{1/2} + O(\lambda_1/\lambda_2)] \ , \tag{B7}$$

and

$$\beta\tilde{\epsilon}_0(\eta) = -\lambda_1(|\eta| + 1/8|\eta|) - (1/2)\ln(2\pi/\lambda_2) + (|\eta| - 1/16|\eta|)^{1/2}(\lambda_1/\lambda_2)^{1/2} + O(\lambda_1/\lambda_2) \ . \tag{B8}$$

Compare Eq. (B6) to Eq. (5.1). The similarity between the results obtained directly from Eq. (4.20) and those

obtained from the differential-equation (4.24) approach, confirm the validity of this last procedure at low temperatures.

The normalization condition yields

$$|\chi(0)|^2=\sqrt{2}[\pi\lambda_1\lambda_2(|\eta|-1/16|\eta|)]^{1/4}e^{\lambda_1(|\eta|+1/8|\eta|)} . \tag{B9}$$

---

*On leave from IMAF, Universidad Nacional de Córdoba, Laprida 854, 5000-Córdoba, Argentina.

[1]N. Gupta and B. Sutherland, Phys. Rev. A 14, 1790 (1976).

[2]R. A. Guyer and M. D. Miller, Phys. Rev. A 17, 1205 (1978).

[3]R. A. Guyer and M. D. Miller, Phys. Rev. A 17, 1774 (1978).

[4]J. F. Currie *et al.*, Phys. Rev. B 22, 477 (1980).

[5]J. F. Currie, M. B. Fogel, and F. L. Palmer, Phys. Rev. A 16, 736 (1977).

[6]J. L. Skinner and P. G. Wolynes, J. Chem. Phys. 73, 4015 (1980).

[7]K. Maki and P. Kumar, Phys. Rev. B 14, 118 (1976); 14, 3920 (1976).

[8]R. K. Dodd, R. K. Bullough, and S. Duckworth, J. Phys. A 8, L64 (1975).

[9]M. Remoissenet, J. Phys. C 14, L335 (1981).

[10]A. C. Scott, F. Y. E. Chu, and D. W. McLaughlin, Proc. IEEE 61, 1443 (1973).

[11]P. W. Kitchenside, A. L. Mason, R. K. Bullough, and P. J. Caudrey, in *Solitons and Condensed Matter Physics,* edited by A. R. Bishop and T. Schneider (Springer, Berlin, 1978); R. K. Bullough, in *Nonlinear Equations in Physics and Mathematics,* edited by A. O. Barut (Reidel, Dordrecht, Holland, 1978).

[12]J. Shiefman and P. Kumar, Phys. Scr. 20, 435 (1979).

[13]M. Büttiker and R. Landauer, Phys. Rev. Lett. 43, 1453 (1979); Phys. Rev. A 23, 1397 (1981).

[14]A. L. Mason, in *Nonlinear Equations in Physics and Mathematics,* edited by A. O. Barut (Reidel, Dordrecht, Holland, 1978).

[15]D. J. Scalapino, M. Sears, and R. A. Ferrell, Phys. Rev. B 6, 3409 (1972).

[16]J. A. Krumhansl and J. R. Schrieffer, Phys. Rev. B 11, 3535 (1974).

[17]R. M. deLeonardis and S. E. Trullinger, Phys. Rev. A 20, 2603 (1979).

[18]S. E. Trullinger *et al.*, Phys. Rev. Lett. 40, 206 (1978); 40, 1603 (1978).

[19]See Figs. 6 and 9 in Ref. 3.

[20]If the system is polarized, then $\langle\theta\rangle\neq 0$. This will certainly be the case whenever $\alpha\neq 0$. For $\eta > -0.25$ the polarization of the DSG chain is only weakly temperature dependent with $\langle\theta\rangle\sim O(\alpha)$. For $\eta < -0.25$, however, at low temperatures the chain tries to reside in the $\theta\neq 0$ potential minima; thus, we find $\langle\theta\rangle\sim O(1)$. We refer to this latter possibility as strong polarization.